Advances in Concrete Construction, *Vol. 8, No. 4 (2019) 335-349*
DOI: https://doi.org/10.12989/acc.2019.8.4.335

Compressive performance of RAC filled GFRP tube-profile steel composite columns under axial loads

Hui Ma*[1,2], Hengyu Bai[1], Yanli Zhao[3], Yunhe Liu[1,2] and Peng Zhang[1]

[1]*School of Civil Engineering and Architecture, Xi'an University of Technology, Xi'an, 710048, China*
[2]*State Key Laboratory of Eco-hydraulics in Northwest Arid Region, Xi'an University of Technology, Xi'an, 710048, China*
[3]*School of Architecture, Chang'an University, Xi'an, 710064, China*

(*Received January 15, 2019, Revised September 4, 2019, Accepted September 15, 2019*)

Abstract. To investigate the axial compressive performance of the recycled aggregate concrete (RAC) filled glass fiber reinforced polymer (GFRP) tube and profile steel composite columns, static loading tests were carried out on 18 specimens under axial loads in this study, including 7 RAC filled GFRP tube columns and 11 RAC filled GFRP tube-profile steel composite columns. The design parameters include recycled coarse aggregate (RCA) replacement percentage, profile steel ratio, slenderness ratio and RAC strength. The failure process, failure modes, axial stress-strain curves, strain development and axial bearing capacity of all specimens were mainly analyzed in detail. The experimental results show that the GFRP tube had strong restraint ability to RAC material and the profile steel could improve the axial compressive performance of the columns. The failure modes of the columns can be summarized as follow: the profile steel in the composite columns yielded first, then the internal RAC material was crushed, and finally the fiberglass of the external GFRP tube was seriously torn, resulting in the final failure of columns. The axial bearing capacity of the columns decreased with the increase of RCA replacement percentage and the maximum decreasing amplitude was 11.10%. In addition, the slenderness ratio had an adverse effect on the axial bearing capacity of the columns. However, the strength of the RAC material could effectively improve the axial bearing capacity of the columns, but their deformability decreased. In addition, the increasing profile steel ratio contributed to the axial compressive capacity of the composite columns. Based on the above analysis, a formula for calculating the bearing capacity of composite columns under axial compression load is proposed, and the adverse effects of slenderness ratio and RCA replacement percentage are considered.

Keywords: recycled aggregate concrete; GFRP tube; profiles steel; composite column; axial compression behavior

1. Introduction

Recycled aggregate concrete (RAC) can effectively utilize recycled coarse aggregate (RCA) made from the abandoned concrete, which is a green building material (Tabsh and Abdelfatah 2009, Zeng *et al*. 2018, Liang *et al*. 2018, Xiong *et al*. 2018, Thomas *et al*. 2013). The present research findings show that the physical properties of RAC material and its structure and structural members are generally not as excellent as those of ordinary concrete (Xiao *et al*. 2012, Rosado *et al*. 2017, Cardoso *et al*. 2016). It is mainly reflected in strength, creep resistance and durability inferior to ordinary concrete (Senaratne *et al*. 2017, Zhang and Zhao 2014, Li *et al*. 2015, Qian *et al*. 2006). Therefore, how to improve the performances of RAC structures is one of the problems that need to be solved at present. In addition, the fiber reinforced polymer (FRP) as a type of composite material (Mesbah and Benzaid 2017, Gulsan, Al Jawahery and Alshawaf 2018) has been used widely in civil engineering because the composite material has many advantages, such as light weight, high temperature resistance, corrosion resistance, creep resistance and the similar coefficient of the thermal expansion to concrete material (Kara 2016, Yao and Teng 2003, Mykolas *et al*. 2013, Desprez *et al*. 2013). As one of those, the glass fiber reinforced polymer (GFRP) constrained concrete structures and structural members are a typical application (Youssef *et al*. 2017, Li and Wu 2015, Zeng *et al*. 2017, Hadi *et al*. 2015).

In recent years, some researchers also proposed GFRP tube constrained recycled aggregate concrete (RAC) columns (Xu *et al*. 2017, Xiao and Huang 2012), which not only obviously improved the mechanical properties of RAC in the columns owing to the restraining effect of GFRP tube, but also was just consistent with the concept of green development. It provides a way for the application of RAC materials in the structures. Many previous studies showed that the GFRP tube constrained RAC columns have high bearing capacity and stiffness, but the corresponding deformability was relatively poor because both RAC and GFRP tubes were all brittle materials. As is known to all, the steel and concrete composite structures, such as the steel reinforced concrete (SRC) structures (Chen *et al*. 2016, Ma *et al*. 2016, Hosseinpour and Abdelnaby 2017), were widely applied in engineering structures due to their advantages of high bearing capacity and ductility. However, it needs to configure steel-rebar skeleton and support template in SRC structures, which means that the construction was relatively

*Corresponding author, Associate Professor
E-mail: mahuiwell@163.com

ISSN: 2287-5301 (Print), 2287-531X (Online)

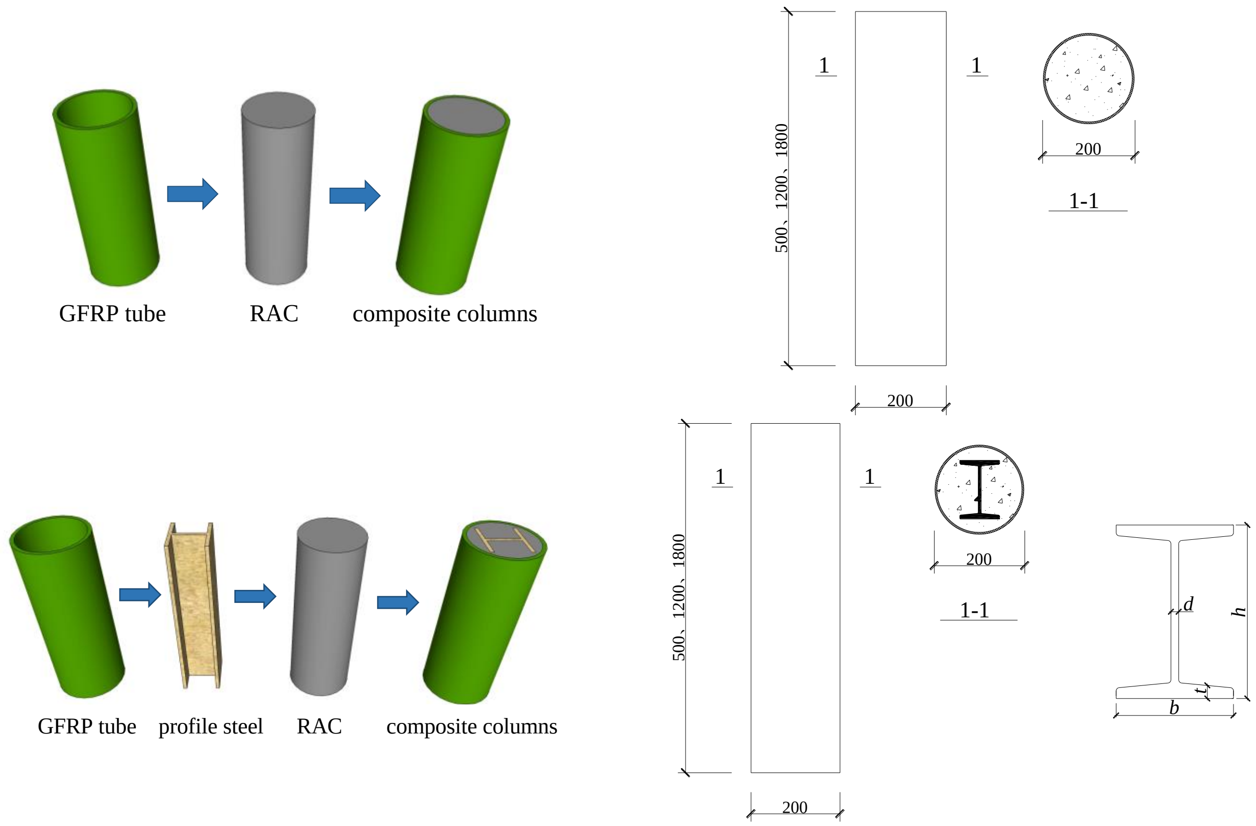

Fig. 1 Design and geometric sizes of the composite columns

Fig. 2 Recycled coarse aggregate (RCA)

Fig. 3 Natural coarse aggregate (NCA)

complicated. In view of this, combining the performance advantages of GFRP tube confined RAC material and SRC structures, a new type of the RAC filled GFRP tube-profile steel composite column is proposed by the authors.

The above composite column has the following advantages. Firstly, the GFRP tube in the composite columns acts as a light weight template and the construction of composite columns can be simplified. Secondly, the external GFRP tube has strong restraint to the internal RAC material, so that the RAC material is in a three-dimensional stress state and the lateral deformation as well as the crack development of RAC material is also limited obviously. In addition, the profile steel in the column can also effectively improve its bearing capacity and deformability. Obviously, the RAC filled GFRP tube-profile steel composite column not only has the advantages of high bearing capacity and stiffness, but also has the characteristics of green buildings. So far, there is little research on the mechanical properties of the above columns. Therefore, the research on the mechanical performance of the columns needs to be carried out.

In this study, the axial compressive behavior of 7 RAC filled GFRP tube columns and 11 RAC filled GFRP tube-profile steel composite columns were investigated under the static loading tests. The failure process, failure modes and the effect of design parameters on the mechanical behavior such as the axial stress-strain curves, strain development and axial bearing capacity of the composite columns under axial compression were analyzed in detail. In addition, the calculation formula of axial bearing capacity of the columns was also put forward by using the superposition method, which can provide the technical reference for the engineering application of this kind of structural members.

2. Axial compression tests of specimens

Table1 Parameters design of specimens for the composite columns

Specimen number	RAC strength grade	RCA replacement percentage r	Column height H/mm	Slenderness ratio λ	section steel ratio ρ
GRC1	C40	0	500	10	-
GRC2	C40	30%	500	10	-
GRC3	C40	50%	500	10	-
GRC4	C40	70%	500	10	-
GRC5	C40	100%	500	10	-
GRC6	C40	100%	1200	24	-
GRC7	C40	100%	1800	36	-
GSRC1	C40	0	500	10	4.54%
GSRC2	C40	30%	500	10	4.54%
GSRC3	C40	50%	500	10	4.54%
GSRC4	C40	70%	500	10	4.54%
GSRC5	C40	100%	500	10	4.54%
GSRC6	C40	100%	500	10	5.76%
GSRC7	C40	100%	500	10	6.85%
GSRC8	C40	100%	1200	24	4.54%
GSRC9	C40	100%	1800	36	4.54%
GSRC10	C50	100%	500	10	4.54%
GSRC11	C60	100%	500	10	4.54%

Table 2 Mix proportion of RAC material

RAC strength grade	RCA replacement percentage r	Water-binder ratio W/B	Weight per unit volume/(kg/m^3)						
			NCA	RCA	Sand	Water	Cement	Fly ash	Water reducer
C40	0	0.440	1171	0	576	195.0	443	0	0
	30%	0.448	819.5	351.3	576	198.5	443	0	0
	50%	0.453	585.5	585.5	576	200.8	443	0	0
	70%	0.459	351.3	819.7	576	203.2	443	0	0
	100%	0.467	0	1171	576	206.7	443	0	0
C50	100%	0.361	0	1138	649	163.0	358	94.0	3.5
C60	100%	0.312	0	1072	528	164.5	422	105.4	6.3

2.1 Design and fabrication of specimens

In the tests, a total of 18 composite column specimens were designed and manufactured, including 7 RAC filled GFRP tube columns and 11 RAC filled GFRP tube-profile steel composite columns. The main design parameters of specimens include the RCA replacement percentage, RAC strength, slenderness ratio and profile steel ratio. Table 1 lists the main design parameters for the above columns. The GFRP material provided by a specialized business company mainly consists of epoxy resin and glass fiber. The epoxy resin matrix connects the glass fibers into a single body, which makes the fibers to be evenly loaded and bear the load together. The diameter of the GFRP tube was 200 mm and its wall thickness was 10 mm. The yield tensile strength and axial compressive strength of the GFRP tube were 350 MPa and 68 MPa, respectively. The longitudinal elastic modulus and hoop elastic modulus of the GFRP tube were 2.1 GPa and 22 GPa, respectively. The profile steel used for the columns was Q235 ordinary carbon steel. Fig. 1 illustrates the design sizes and cross section of the specimens, which included the RAC filled GFRP tube columns and the RAC filled GFRP tube-profile steel composite columns.

Table 3 Basic physical performances of RAC material

RAC strength grade	RCA replacement Percentage r	Cube compressive strength f_{rcu}/MPa	Prismatic axial compressive strength f_{rc}/ MPa	Elastic modulus E_s/MPa
C40	0	43.37	32.96	2.685×10^4
C40	30%	43.26	32.88	2.683×10^4
C40	50%	42.26	32.12	2.667×10^4
C40	70%	41.38	31.45	2.653×10^4
C40	100%	40.01	30.41	2.630×10^4
C50	100%	51.61	39.22	2.796×10^4
C60	100%	61.58	46.80	2.898×10^4

Table 4 Physical dimension and basic physical performances of steel products

Type of profile steel	Height h /mm	Width b/mm	Web thickness d /mm	Flange thickness t/mm	Area s/mm^2
Number 10	100	68	4.5	7.6	143000
Number 12.6	126	74	5.0	8.4	181000
Number 14	140	80	5.5	9.1	215000

Steel type		Yield strength f_y/MPa	Ultimate strength f_u/MPa	Elastic modulus E_s/MPa
Profile steel	Flange	327.6	459.7	2.02×10^5
	Web	339.2	467.6	1.97×10^5

The recycled coarse aggregate (RCA) material in the tests came from the concrete of demolished old buildings, as shown in Fig. 2. The continuous grading for the particle size of the RCA was 5-25 mm in the RAC material. The basic mechanical performances of these RCA used in the columns can conform to the basic requirements of Chinese Specification of GB/T- 25177- 2010 for recycled coarse aggregate for concrete. In addition, the natural coarse aggregate (NCA) adopted for the columns was artificial gravel broken from the natural stone, as shown in Fig. 3. The river sand with good grading was adopted as fine aggregate in the RAC material. In addition, the ordinary Portland cement was used as the cementitious materials and its strength grade was R42.5. The design of mix proportion and basic mechanical properties of RAC material are listed in Tables 2 and 3, respectively. The size and mechanical properties of steel products used in the composite columns are given in Table 4.

In the RAC filled GFRP tube-profile steel composite columns, the upper and lower steel plates in the columns were used to fix the position of the internal profile steel and GFRP tubes with a silicone rubber adhesive. In addition, the upper and lower steel plates were also used to transfer the axial compression loads uniformly in the tests. In addition, the amount of each component of RAC materials in the composite columns can be calculated according to their mix proportions. During the pouring process, the internal RAC in the specimens was uniformly vibrated with a portable vibrator, which made the RAC materials in the columns as compact as possible. The main making process

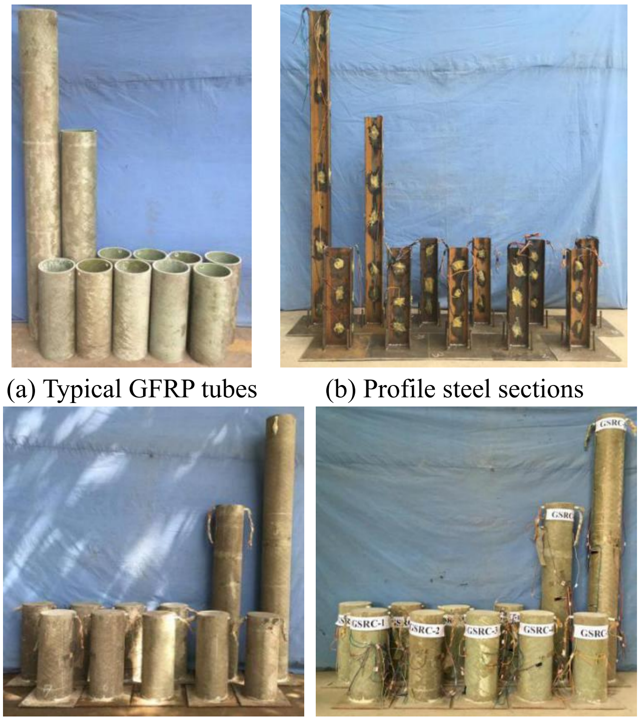

(a) Typical GFRP tubes (b) Profile steel sections

(c) Typical composite columns

Fig. 4 Main making process of the composite columns

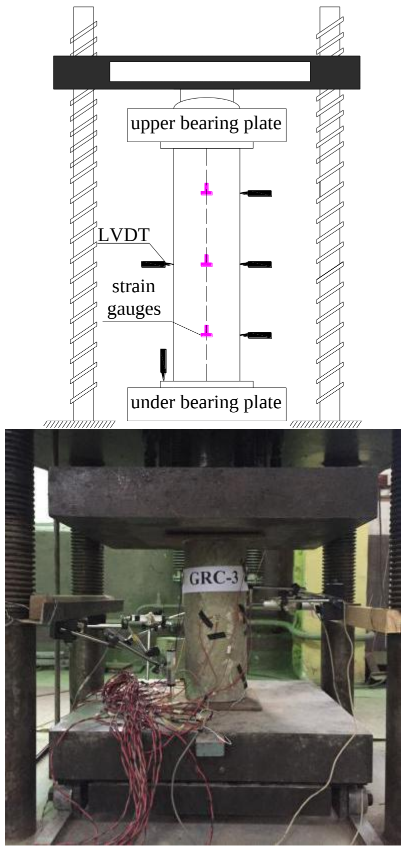

Fig. 5 Test devices of the composite columns under axial compression loads

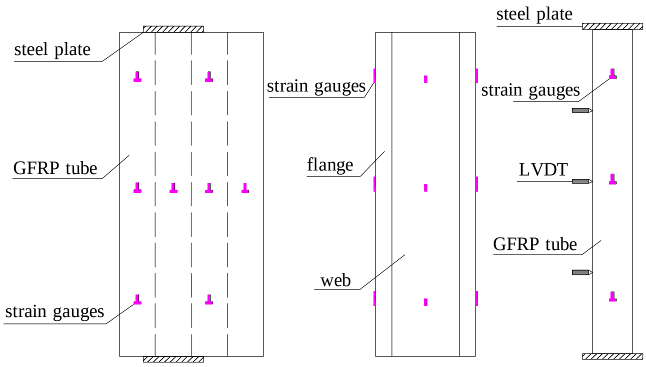

Fig. 6 Measuring points of strains and displacements of the composite columns

of specimens is exhibited in Fig. 3.

2.2 Test devices and loading methods

A 500t elector-hydraulic servo testing machine in the Structural Engineering Laboratory at Xi'an University of Technology was used to carry out the static tests on the specimens under the axial compression loads. The test devices in this study are illustrated in Fig. 5. The loading procedure of specimens including the force loading stage and displacement loading stage was adopted in the test. Firstly, the pre-loading was applied onto the columns, so as to eliminate the gap between the specimen and the loading end plate. Subsequently, the testing machine was unloaded to zero and the formal loading was applied onto the columns according to the loading procedure. The load control was used before the load reached $0.6P_{max}$ (i.e., P_{max} was the predicted value of the peak load), and the load gradually increased by $P_{max}/12$ per level. After $0.6P_{max}$, the displacement control was applied to the compsoite columns and the loading rate was maintained at 1.5 mm/min. Finally, when the specimens were damaged or unsuitable for the further loading, the test was finished.

In the axial compression tests, the applied loads and the data acquisition were synchronized in the loading process. The axial load-displacement curves of the specimens were automatically obtained through the computer. The displacement and deformations at important positions of the specimens were measured by using the displacement transducers. Fig. 5 illustrates the positions of displacement transducers in the tests, which were set at the upper, middle, lower and bottom plate positions of the specimens. In addition, the strain developments on the GFRP tube and profile steel in the specimens were measured by arranging the longitudinal and transverse strain gauges. The strain gauges were also set at the upper, middle and lower of the GFRP tube and profile steel, respectively, as shown in Fig. 6. The wires of the strain gauges on the profile steel of specimens were connected to the acquisition instrument through a reserved hole in the GFRP tube.

3. Main test results

3.1 Failure process and failure modes

Based on the careful observations of the tests, the failure

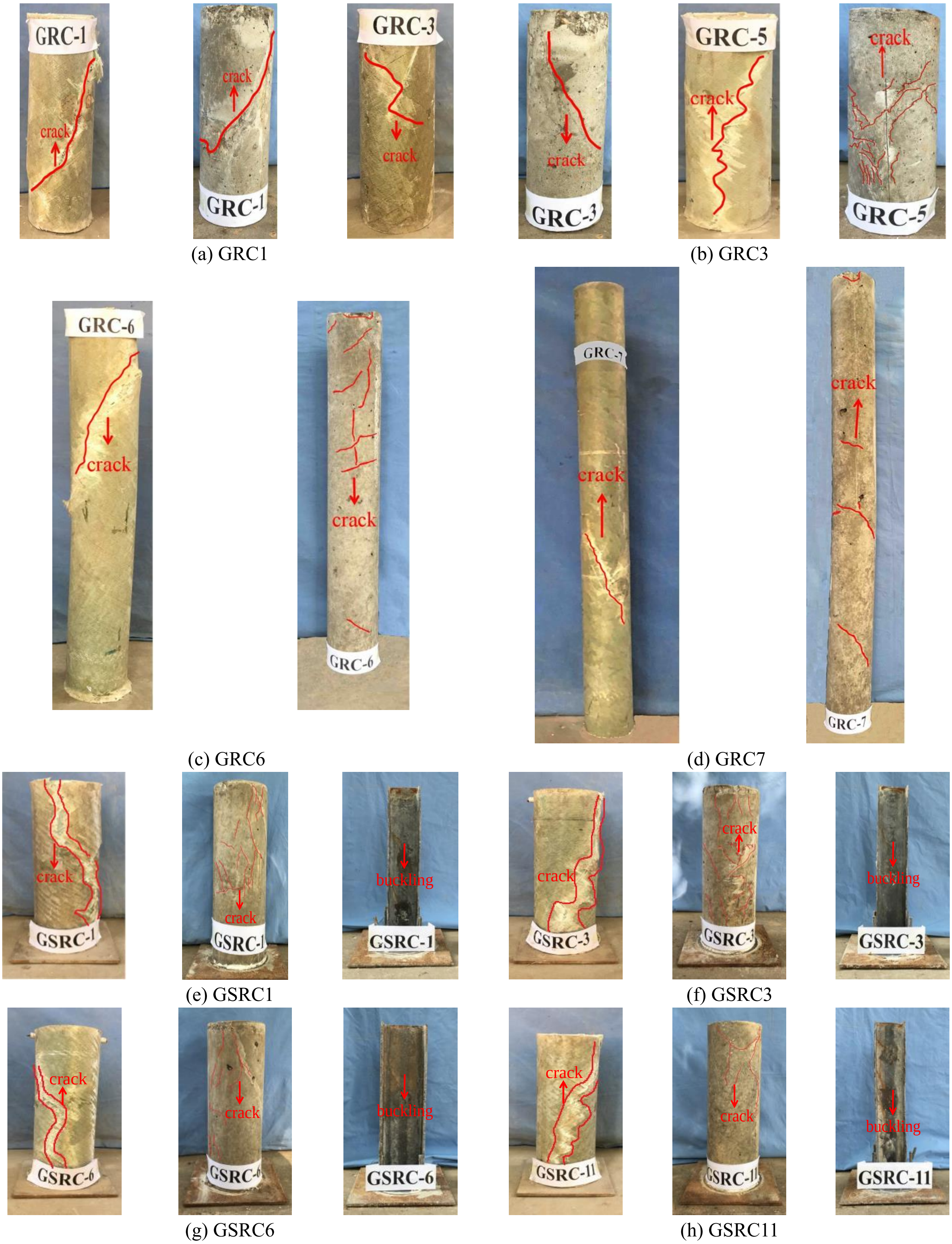

Fig. 7 Failure modes of typical column specimens

modes of the short and long columns under axial compression loads had some differences. Therefore, the failure process and failure modes of the short and long columns in the tests are described separately. The typical failure modes of the RAC filled GFRP tube columns and RAC filled GFRP tube-profile steel composite columns are

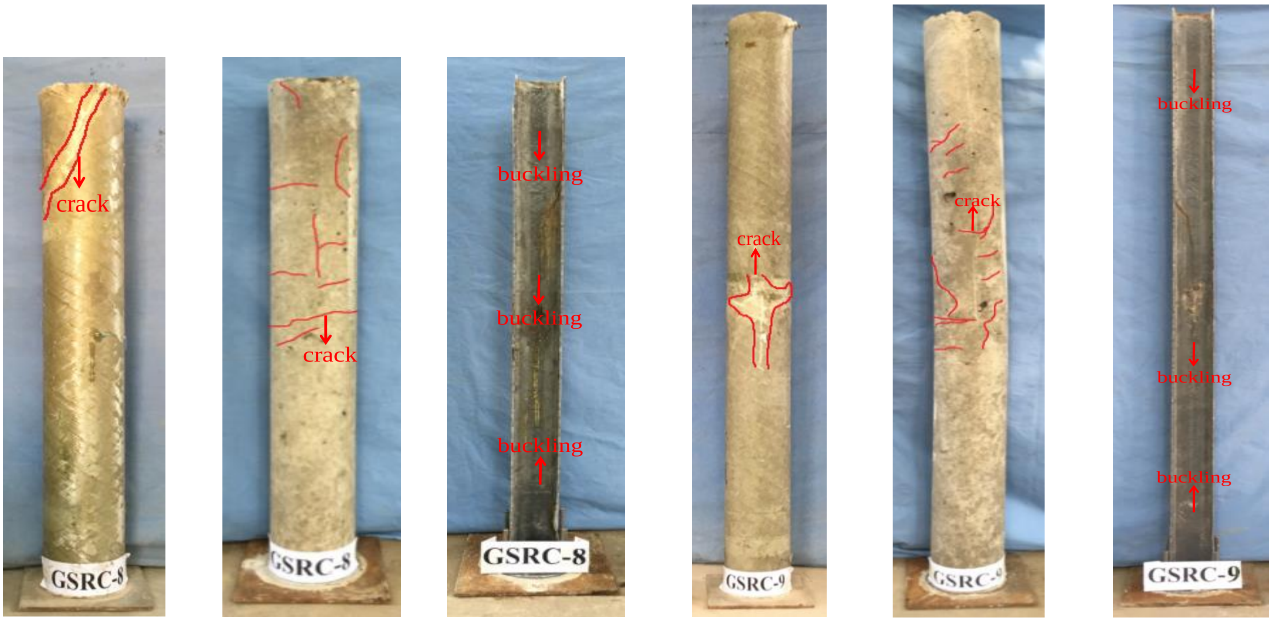

(e) GSRC8 (f) GSRC9

Fig. 7 Continued

illustrated in Fig. 7.

3.1.1 GRC1-GRC7 composite columns

In the RAC filled GFRP tube columns, the failure process and failure modes of GRC1-GRC7 specimens under axial compression loads were relatively similar. In the initial loading stage, the specimens were in the elastic state and the deformation of the specimens was very small. The GFRP tube and RAC sustained the loads respectively. This indicates that the restraint effect of the GFRP tube on the RAC material was very small. When the axial compression load increased to about 60% of the ultimate load, the relationship between the axial compression load and deformation became nonlinear, which means that the specimens entered the elastic-plastic stage. As the axial load continued to increase, the fiberglass of the GFRP tube wall began to slightly tear with a little noise. At this time, the transverse deformation of the internal RAC increased, resulting in the increase of the radial pressure between the RAC and GFRP tube, which also shows the RAC was obviously restrained by the GFRP tube. When the load increased to 70%~80% of the ultimate load, the middle area of specimens bulged slightly and the lateral deformation of specimens increased obviously. In addition, the lateral deformations of GRC6 and GRC7 specimens (i.e., middle long columns) were larger than those of GRC1-GRC5 specimens (i.e., short columns). Meanwhile, there was a slight white stripe around the surface of the GFRP tube, and the sound of tearing on fiberglass became bigger. The overall axial compression deformation of the specimens increased and the corresponding stiffness decreased gradually. When the load reached 80% to 90% of the ultimate load, the specimens emitted a continuous sound of tearing on GFRP, and the white fringes around the GFRP tube wall overlapped more and more. In the meantime, there is a small sound of crushing on the RAC inside the specimen. The greater the transverse deformation of the RAC, the greater the circumferential stress of the GFRP tube, so the greater the restraint stress on the RAC. When the load reached the ultimate load, the fibers in the middle of the GFRP tube were broken first and then extended to both sides. With the further increase of load, the tearing failure on the GFRP tube was formed at a certain location, accompanied by a huge sound. The RAC in the GFRP tube was crushed, and the column specimens lost its axial bearing capacity.

3.1.2 GSRC1-GSRC11 specimens

In the RAC filled GFRP tube-profile steel composite columns, GSRC1-GSRC7 and GSRC10-GSRC11 specimens were short columns and GSRC8-GSRC9 specimens were medium and long columns. During the initial stage of loading, the axial deformation of the specimens was not obvious and increased linearly with the increase of loads. In the short columns, when the loads increased to 60% of the peak loads, the axial compressive deformation began to appear on the specimens accompanied by a slight noise. In the medium-long columns, when the axial loads advanced to about 50% of the peak loads, the axial deformation of the specimens was enhanced obviously. Because part of the glass fiber was slightly torn, the matrix resin began to sustain tensile stress. Meanwhile, in the short columns, the middle part of the GFRP tube's surface became slightly irregular whitening. When the axial compression load reached 80% of the peak load, the axial deformation of the specimens increased obviously, and there was slight bulging deformation accompanied by the louder fracture sound from the glass fiber in the middle part of the medium-long column. In addition, the RAC in the columns cracked and the stiffness degradation of the columns became obvious. When the axial loads advanced closely to the peak loads, there was a sustained fiber

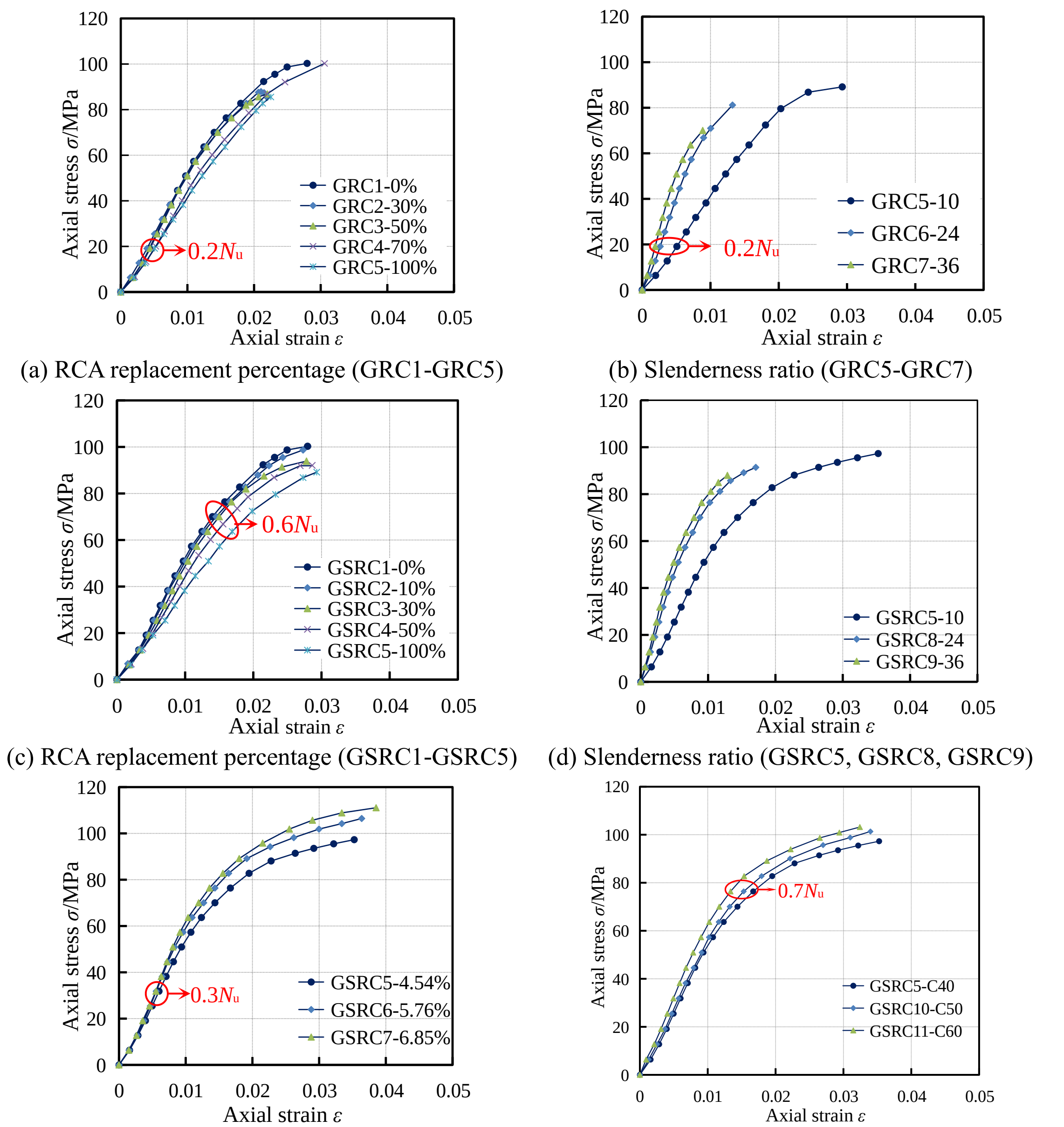

(a) RCA replacement percentage (GRC1-GRC5) (b) Slenderness ratio (GRC5-GRC7)

(c) RCA replacement percentage (GSRC1-GSRC5) (d) Slenderness ratio (GSRC5, GSRC8, GSRC9)

(e) Profile steel ratio (GSRC5-GSRC7) (f) RAC strength grade (GSRC5, GSRC10, GSRC11)

Fig. 8 Axial stress-strain curves of the composite columns with different design parameters

breakage sound in the columns. The tearing of glass fiber became serious and the matrix resin was pulled to produce the obvious phenomenon of stress whitening in the GFRP tube. After the peak load, the large diagonal cracks formed in the GFRP tube because of the tearing of glass fiber with the increase of loads. Subsequently, the specimen lost its axial bearing capacity. After the test, the GFRP tube was cut along its longitudinal direction. It was found that there were many irregular cracks in the internal RAC and the upper part of profile steel had local buckling deformation. This indicated that the profile steel had already yielded before the failure of the composite columns.

Through the above analysis and compared with the RAC filled GFRP tube columns, obviously, the axial bearing capacity and deformation capacity of the RAC filled GFRP tube-profile steel composite columns had been improved significantly. Based on Table 5, in terms of axial bearing capacity and deformation, compared with the RAC filled GFRP tube columns, the maximum increases for the RAC filled GFRP tube profile steel short composite columns were 10.9% and 25.8%, respectively. In the medium-long columns, the above-mentioned values were 25.7% and 45.1%, respectively.

3.2 Axial stress-strain relationships of the columns

Fig. 8 illustrates the axial stress-strain curves of specimens obtained from the axial compression tests and Table 5 describes the test values of the specimens under axial compression loads. From Fig. 8(a)-(f) and Table 5, the influence of the design parameters on the axial stress-strain curves and the test results of the composite columns can be described as follows:

(1) Fig. 8(a) and (c) show the influence of RAC

Table 5 Test results of the composite columns

Specimen number	RAC strength grade	RCA replacement percentage *r*	Column height *H*/mm	Slenderness ratio *λ*	section steel ratio *ρ*	(Peak load)/kN	(Peak displacement) /mm
GRC1	C40	0	500	10	-	3150.65	13.98
GRC2	C40	30%	500	10	-	3100.58	13.65
GRC3	C40	50%	500	10	-	2950.35	13.90
GRC4	C40	70%	500	10	-	2892.98	14.32
GRC5	C40	100%	500	10	-	2801.00	14.65
GRC6	C40	100%	1200	24	-	2550.12	15.87
GRC7	C40	100%	1800	36	-	2200.16	15.96
GSRC1	C40	0	500	10	4.54%	3387.75	17.58
GSRC2	C40	30%	500	10	4.54%	3301.99	17.00
GSRC3	C40	50%	500	10	4.54%	3270.54	17.10
GSRC4	C40	70%	500	10	4.54%	3010.04	12.37
GSRC5	C40	100%	500	10	4.54%	3056.58	17.63
GSRC6	C40	100%	500	10	5.76%	3343.74	18.19
GSRC7	C40	100%	500	10	6.85%	3489.74	19.27
GSRC8	C40	100%	1200	24	4.54%	2871.67	20.50
GSRC9	C40	100%	1800	36	4.54%	2764.80	23.16
GSRC10	C50	100%	500	10	4.54%	3183.89	16.99
GSRC11	C60	100%	500	10	4.54%	3242.19	16.21

replacement percentage on the axial stress-strain curves of the RAC filled GFRP tube columns and RAC filled GFRP tube-profile steel composite columns under the same strength grades of the RAC, respectively. During the initial loading, the columns were in the elastic state and the relationship between the axial stress and the axial strain was approximately linear. At this stage, the ascending section of the curves was almost overlapping under different RAC replacement percentages, which indicates that the RCA replacement percentage had little influence on the initial stiffness of columns. In the RAC filled GFRP tube columns, when the increase of the axial load to 20% of its peak value, the difference between the curves became obvious gradually and the axial compressive stiffness of columns decreased. In the RAC filled GFRP tube columns-profile steel composite columns, the difference between the curves became obvious gradually until 60% of the peak value was reached. With the increase of RCA replacement percentages, the peak load of the RAC filled GFRP tube columns and RAC filled GFRP tube-profile steel composite columns decreased by 11.1% and 9.8% at most. However, the peak displacement of the RAC filled GFRP tube columns and RAC filled GFRP tube-profile steel composite columns increased by 4.8% and 0.3% at most. It can be seen that RCA replacement percentages had certain adverse effects on the bearing capacity and stiffness of the specimens.

(2) The difference of the axial stress-strain curves of the specimens with different slenderness ratios was shown in Fig. 8(b) and (d). The axial stress-strain curves of the RAC filled GFRP tube columns and RAC filled GFRP tube-profile steel composite columns were relatively similar, but the deformation and stiffness of the GFRP tube-profile steel composite columns are obviously higher than those of the RAC filled GFRP tube columns. Obviously, the axial compressive capacity and stiffness of the columns obviously decreased with the increasing slenderness ratio. In addition, the composite columns with large slenderness ratio have large axial compressive deformation. The peak load of the RAC filled GFRP tube columns and RAC filled GFRP tube-profile steel composite columns decreased by 9.5% and 21.5% at most. Meanwhile, the peak displacement of the RAC filled GFRP tube columns and RAC filled GFRP tube-profile steel composite columns increased by 8.9% and 31.4% at most. Obviously, the second-order effect of axial loads had an adverse effect on the bearing capacity and deformation of long composite columns. Therefore, the slenderness ratio of the columns needs to be controlled, so as to minimize the adverse effects of the second-order effect.

(3) Fig. 8(e) indicates that the stiffness and axial bearing capacity of the RAC filled GFRP tube profile steel composite columns were significantly affected by the profile steel ratio. The axial stress-strain curves of the composite columns with different profile steel ratios were almost coinciding during the initial loading stage. After the load increased to about 30% of the peak load, the axial stress-strain curves became different obviously. In the wake of increased profile steel ratio, the peak loads of columns increased gradually. Furthermore, in the late loading stage, the axial stress-strain curve of the columns with the large steel ratio became gentle, which indicates that the deformation capacity of the columns increased with the increasing steel ratio. In addition, the peak loads of the above composite columns increased by 14.17% at most. Meanwhile, the peak displacement of the composite columns increased by 9.3% at most. Thus, a reasonable design of profile steel ratio was important for this type of

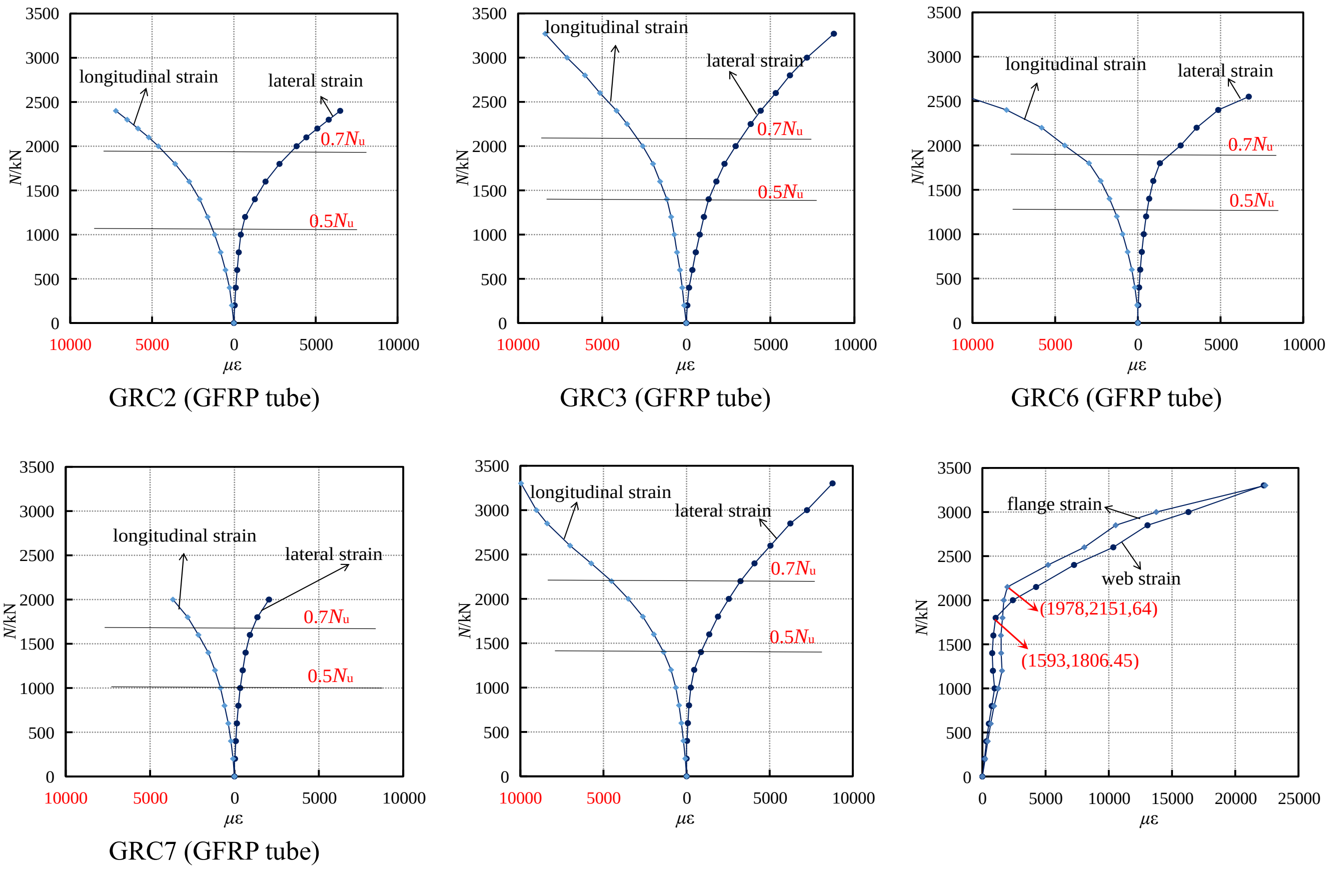

(a) GSRC2 (GFRP tube and profile steel)

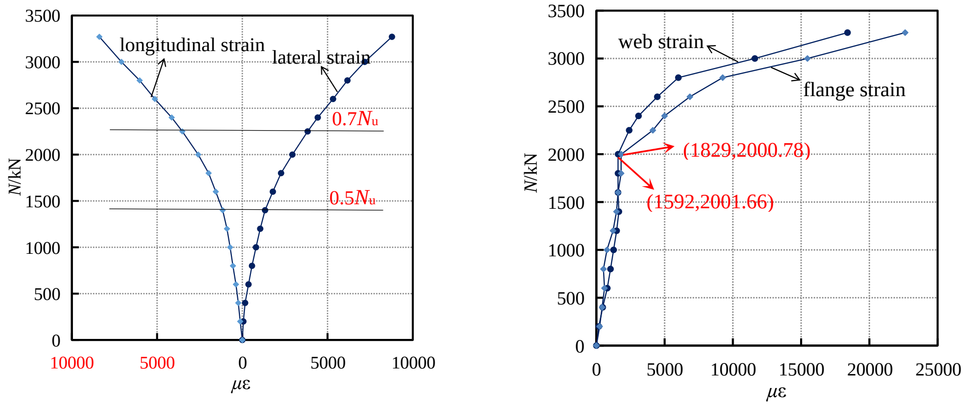

(b) GSRC3 (GFRP tube and profile steel)

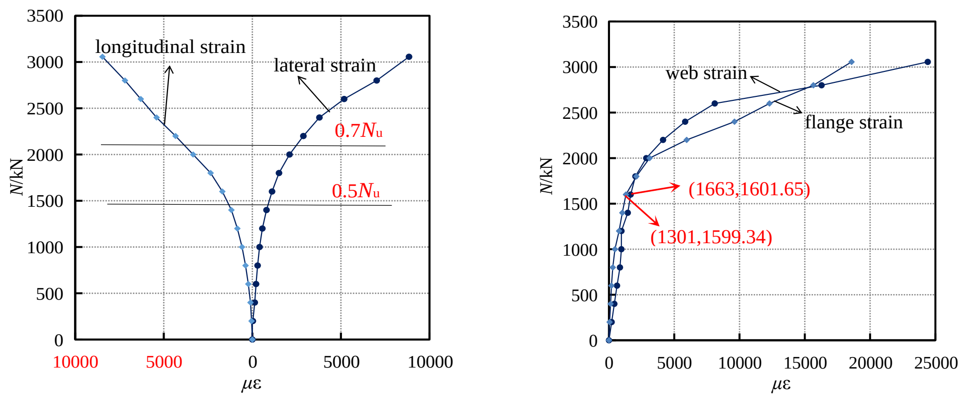

(c) GSRC5 (GFRP tube and profile steel)

Fig. 9 Load-strain curves of typical RAC filled GFRP tube-profile steel columns

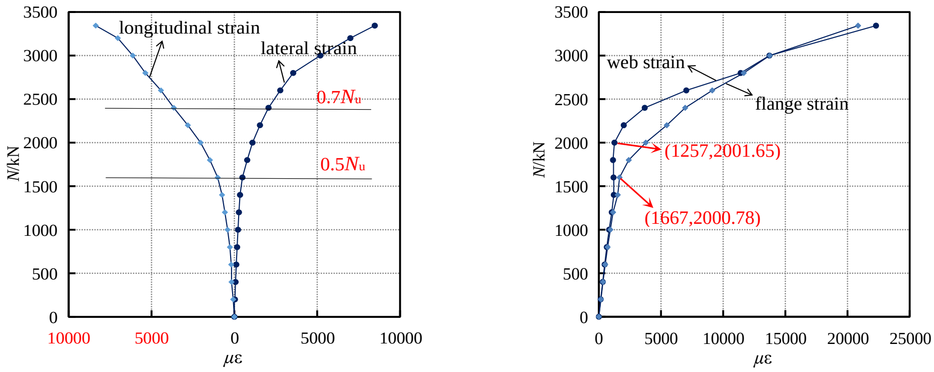

(d) GSRC6 (GFRP tube and profile steel)

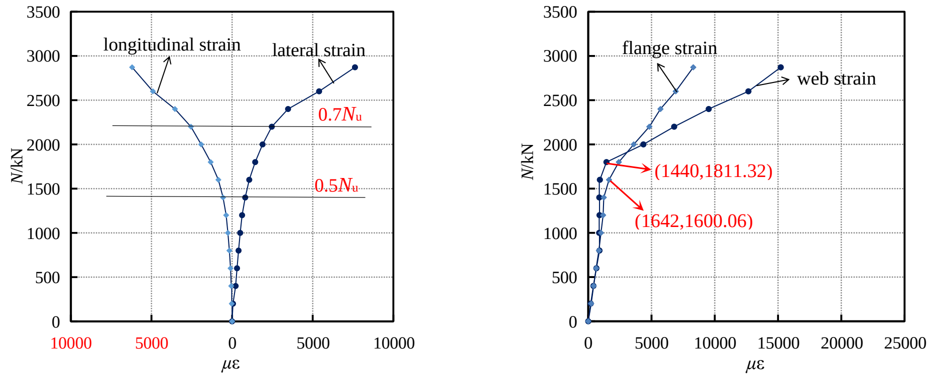

(e) GSRC8 (GFRP tube and profile steel)

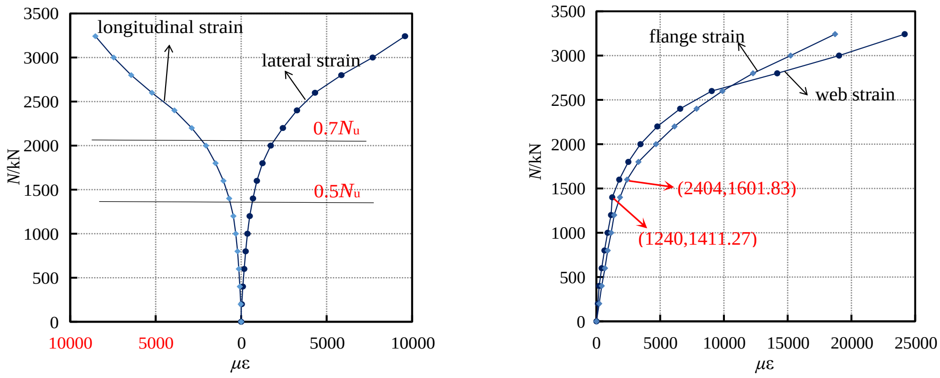

(f) GSRC11 (GFRP tube and profile steel)

Fig. 9 Continued

composite column, which can improve the axial bearing capacity and deformation of the composite columns.

(4) From Fig. 8(f), it can be seen that the axial stress-strain curves of the RAC filled GFRP tube-profile steel composite columns with different RAC strengths had some difference. During the initial loading period, the axial stress-strain curves of the composite columns changed approximately linearly, which indicated that the columns were in the elastic stage. After the axial load reached to 70% of the peak value, the slope of the curves of the composite columns changed greatly. With the increasing RAC strength, the slope of the curves of composite columns increased to a certain extent. In addition, the peak loads of the above composite columns can increase by 6.1% at most. Meanwhile, the peak displacement of composite columns decreased by 8.1% at most. This means that the axial bearing capacity and stiffness of the columns increased gradually with the increasing RAC strength, but the deformability was relatively reduced.

3.3 Strains of the GFRP tube and profile steel

The strain curves of GFRP tube and profile steel in the specimens can be measured by using the strain gauges attached at the measuring points. The basic shapes and trends of the load-strain curves of the GFRP tube and profile steel in the all specimens were basically similar. Based on the test data, Fig. 9 reveals the strain characteristics of the GFRP tube and profile steel of typical specimens.

Based on Fig. 9, in the RAC filled GFRP tube columns and RAC filled GFRP tube-profile steel composite columns, the longitudinal strains and hoop strains of the GFRP tubes both increased linearly and were in elastic state during the initial phase of loading. This means that the constraint influence of the GFRP tube on the internal RAC was relatively small at this stage. In the RAC filled GFRP tube columns, such as GRC2, when the axial load increased to about 50% of the peak load, the longitudinal and circumferential strains of the GFRP tube in the column were 1966.5 $\mu\varepsilon$ and 1130.8 $\mu\varepsilon$, respectively, and increased rapidly. When the axial load increased to about 70% of the peak load, the longitudinal and circumferential strains of the GFRP tube in the column were 3793.6 $\mu\varepsilon$ and 3307 $\mu\varepsilon$, respectively. Obviously, the growth rate of the circumferential strain of the GFRP tube is obviously greater than that of the longitudinal strain, which indicates that the restraint ability of GFRP tube to the internal RAC is obviously enhanced, and the crack propagation is restricted.

Similarly, in the RAC filled GFRP tube-profile steel composite columns, such as GSRC2 specimen, when the axial load increased to about 50% of the peak load, the longitudinal and circumferential strains of the GFRP tube were 2133.0 $\mu\varepsilon$ and 1495.3 $\mu\varepsilon$, respectively. When the axial load increased to about 70% of the peak load, the longitudinal and circumferential strains of the GFRP tube were 5125.0 $\mu\varepsilon$ and 3665.0 $\mu\varepsilon$, respectively. The above analysis shows that the GFRP tube can effectively restrain the internal RAC. After the tearing of glass fibers in the GFRP tube, the constraint effect was weakened due to the tearing of glass fibers and the transverse deformation of glass fibers rapidly increased until the glass fiber tube lost its axial bearing capacity.

In addition, during the initial loading stage, the load-strain curves of the profile steel in the RAC filled GFRP tube-profile steel composite columns were also basically linear. For example, in GSRC2 specimen, when the axial compressive load increased to 50% of the peak load, the longitudinal strains of the web and flange of the profile steel were 914.5 $\mu\varepsilon$ and 1498.5 $\mu\varepsilon$, respectively. The curves of the profile steel began to change nonlinearly and the growth rate of its strain increased rapidly. With the increase of axial loads, the profile steel in the columns basically reached its yield stress. At this point, the longitudinal strains of the web and flange of the profile steel were 1593.0 $\mu\varepsilon$ and 1798.0 $\mu\varepsilon$, respectively. Subsequently, when the axial load continued to increase, the strain of the profile steel increased sharply, which shows that the profile steel had been fully utilized. When the axial load of composite column was close to the peak load, the profile steel had completely yielded.

Comparing to the load-strain curves of the GFRP tube and profile steel in the composite columns shows that the development rate of the strain of the profile steel was obviously faster than that of the GFRP tube. This means that the profile steel first reached yield stress and then the RAC was crushed as well as the glass fiber tube was torn gradually until the failure of the column occurred. This type of failure mode can make good use of the mechanical properties of the profile steel and GFRP tube in this kind of column. More importantly, the mechanical properties of the RAC material in the composite columns were significantly improved by the restraint effect of the GFRP tube. Based on the comparative analysis, the axial bearing capacity and deformation capacity of the RAC filled GFRP tube-profile steel composite columns are obviously higher than those of the RAC filled GFRP tube columns.

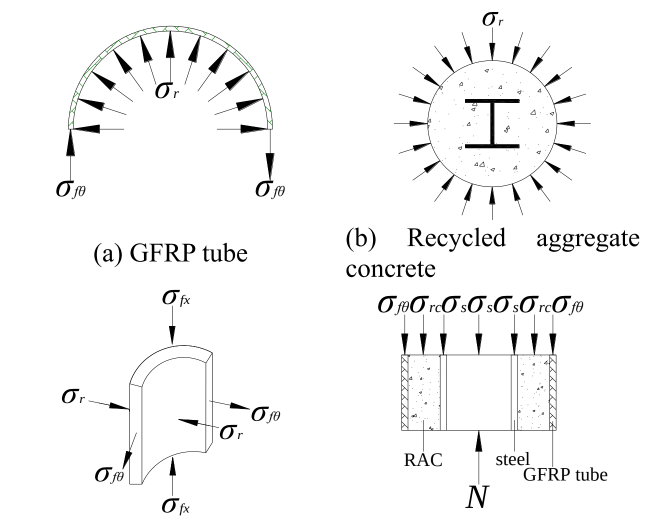

Fig. 10 Axial compression mechanism of the composite columns

4. Calculation on the axial bearing capacity of composite columns

4.1 Axial compression mechanism of the columns

Based on the above analysis, the axial bearing capacity of the RAC filled GFRP tube columns was contributed by the GFRP tube and internal RAC together, while the axial bearing capacity of the RAC filled GFRP tube-profile steel composite columns was contributed together by the GFRP tube, internal RAC and profile steel. Obviously, the GFRP tube in the columns had strong restrained effect to the internal RAC material and profile steel. The internal RAC material of the columns was in three-dimensional pressure state under the constraint effect of the GFRP tube, as shown in Fig. 10. This effectively improves the mechanical behavior of the composite columns under axial compression loads. In addition, the radial pressure on the GFRP tube of the columns can be neglected because it was far less than the corresponding circumferential and axial compressive pressures. Therefore, the radial stress of the GFRP tube can be ignored in the calculation process. Fig. 10 describes the loading mechanism of the composite columns under axial compression loads.

4.2 Bearing capacity of the internal RAC

It is considered that the GFRP tube has a restraint force on the internal RAC. According to Fig. 10(a) by the load balance, σ_r can be obtained by

$$\sigma_r = -\frac{2t\sigma_{f\theta}}{d_0} \tag{1}$$

where σ_r is the constraint stress of the GFRP tube, $\sigma_{f\theta}$ is the hoop stress of the GFRP tube, t is the wall thickness of the GFRP tube, and d_0 is the inner diameter of the GFRP tube.

The constraint strength of the GFRP tube can be given by

$$f_r = \frac{2 f_f t}{d_0} \tag{2}$$

where f_f is the binding of the GFRP tube, and f_r is the circumferential tensile strength of the GFRP tube.

The compressive strength of the internal RAC can be improved by the restrained effect of the GFRP tube. It is assumed that f_{fc} is the compressive strength of the RAC confined by the GFRP tube, f_c is the standard value of the axial compressive strength of the RAC, and k is the stress increasing coefficient of the RAC after the restraint. For simplified calculation, according to the case of ordinary concrete, the formula can be given as follow (Samaan and Mirmiran 1998)

$$f_{fc} = f_c + k f_r \tag{3}$$

$$k = 6 f_r^{-0.3} \tag{4}$$

4.3 Bearing capacity of the profile steel

The profile steel in the compsoite columns was subjected to the longitudinal compressive stress and lateral restraining stress, and is in the state of three-dimensional stress. Based on the Von Mises yield condition, the following formula can be derived

$$\frac{1}{2}\left[(\sigma_1-\sigma_2)^2+(\sigma_2-\sigma_3)^2+(\sigma_3-\sigma_1)^2\right]= f_s^2 \tag{5}$$

where σ_1 is the first principal stress, σ_2 is the second principal stress, and σ_3 is the third principal stress.

In addition, the profile steel used in the columns can be assumed to have the same tensile and compressive strengths. From the material mechanics (Yu 2004)

$$\sigma_1 = \sigma_2 = \frac{2t}{d_0-2t} f_r \tag{6}$$

Combining Eqs. (5) and (6) yields

$$\sigma_3 = f_s + \frac{2t}{d_0-2t} f_r \tag{7}$$

Therefore, the strength of the profile steel after being restrained by the GFRP tube can be increased by

$$f_{sr} = f_s + \frac{2t}{d_0-2t} f_f \tag{8}$$

where f_{sr} is the strength of the profile steel by the constraint effect and f_s is the yield strength of the profile steel in the columns.

4.4 Bearing capacity of the GFRP tube

The axial compressive stress corresponding to the end of the strengthening phase of the composite column was taken as the design index of the structural members, and the stress of the GFRP tube at this point can be considered as the ultimate stress.

When the relationship between the axial stress and strain of a composite column develops at the end of the elasto-plastic phase, the GFRP tube is doubly stressed by the axial compression and the radial stretching in the tube at this point. Therefore, the stress-strain relationships of the GFRP tube can be expressed as follow

$$\begin{cases} \varepsilon_{fx} = \dfrac{\sigma_{fx}}{E_{fz}} - \dfrac{v_{f\theta x}\sigma_{f\theta}}{E_{f\theta}} \\ \varepsilon_{f\theta} = \dfrac{\sigma_{f\theta}}{E_{f\theta}} - \dfrac{v_{fx\theta}\sigma_{fx}}{E_{fx}} \end{cases} \tag{9}$$

where $\varepsilon_{f\theta}$ is the hoop strain of the GFRP tube, ε_{fx} is the axial strain of the GFRP tube, $\sigma_{f\theta}$ is the hoop stress of the GFRP tube, σ_{fx} is the axial stress of the GFRP tube, and $v_{f\theta x}$ is the circumferential Poisson's ratio of the GFRP tube.

The axis strain formula of unidirectional plate for the GFRP tube can be given as follow (Kelly and Mileiko 1983)

$$\varepsilon_y = n^2 \varepsilon_T \tag{10}$$

When the ultimate state of the GFRP tube is reached, it is approximately assumed that the strain in the direction of the principal axis of the unidirectional plate is given as follow

$$\varepsilon_T = \varepsilon_{fu} \tag{11}$$

where n is the direction sine of the fiber winding angle of the GFRP tube, ε_T is the strain in the principal axis of the unidirectional plate, ε_y is the strain in the y-axis of the unidirectional plate, and ε_{fu} is the elongation at break in the longitudinal direction of the unidirectional plate.

The circumferential ultimate strain of the GFRP tube can be given follow

$$\varepsilon_{\theta u} = n^2 \varepsilon_{fu} \tag{12}$$

The axial loads of GFRP tube are mainly borne by the resin and the fracture elongation of resin is considered as the axial ultimate strain of the GFRP tube.

The axial compressive deformation occurs when the composite columns is uniformly compressed. Therefore, according to the definition and relation of deformation coordination and Poisson's ratio, the ultimate axial strain of the GFRP tube can be expressed as follows

$$\varepsilon_{xu} = \frac{-\varepsilon_{\theta u}}{\mu_f} \tag{13}$$

where ε_{xu} is the axial ultimate strain of the GFRP tube, $\varepsilon_{\theta u}$ is the circumferential ultimate strain of the GFRP tube, and μ_f is the axial pressure Poisson's ratio of the columns during the strengthening phase.

Therefore, the ultimate compressive strength of the GFRP tubes in the compsoite columns obtained from Eqs. (9) and (13) can be given by

$$f_{fy} = \frac{(1+\mu_f v_{f\theta x})E_f \varepsilon_{\theta u}}{(1-v_{f\theta x} v_f)\mu_f} \tag{14}$$

Table 6 Comparison of the calculated and tested axial compressive capacities of the composite columns

Specimen	RAC strength grade	GFRP tube thickness t/mm	Section steel ratio /ρ	RCA replacement Percentage/r	Slenderness ratio/λ	N_t/kN	N_c/kN	N_c/N_t
GRC1	C40	10	-	0%	10	3150.65	3137.64	0.996
GRC2	C40	10	-	30%	10	3100.58	3032.18	0.978
GRC3	C40	10	-	50%	10	2950.35	2952.63	1.001
GRC4	C40	10	-	70%	10	2892.98	2875.11	0.994
GRC5	C40	10	-	100%	10	2801.00	2759.79	0.985
GRC6	C40	10	-	100%	24	2550.12	2366.66	0.928
GRC7	C40	10	-	100%	36	2200.16	2184.58	0.993
GSRC1	C40	10	4.54	0	10	3387.75	3329.67	0.983
GSRC2	C40	10	4.54	30%	10	3301.99	3222.53	0.976
GSRC3	C40	10	4.54	50%	10	3270.54	3147.89	0.962
GSRC4	C40	10	4.54	70%	10	3010.04	2983.42	0.991
GSRC5	C40	10	4.54	100%	10	3056.58	2975.83	0.974
GSRC6	C40	10	5.76	100%	10	3343.74	3357.31	1.004
GSRC7	C40	10	6.85	100%	10	3489.74	3416.31	0.979
GSRC8	C40	10	4.54	100%	24	2871.67	2703.45	0.941
GSRC9	C40	10	4.54	100%	36	2764.80	2930.70	1.060
GSRC10	C50	10	4.54	100%	10	3183.89	3072.04	0.965
GSRC11	C60	10	4.54	100%	10	3242.19	3299.30	1.018

N_t is the test values of axial bearing capacity; N_c is the calculated values of axial bearing capacity; the average value of N_c/N_t is 0.99; and the standard deviation of N_c/N_t is 0.016.

where E_f is the axial compression modulus of the GFRP tube.

4.5 Axial bearing capacity of the composite columns

Based on the above analysis and formulas, the axial compressive capacity of the RAC filled GFRP tube columns was contributed by two parts in the columns, i.e., the RAC and GFRP tube. Similarly, the axial compressive capacity of the RAC filled GFRP tube-profile steel composite columns was contributed by three parts in the columns, i.e., the RAC, profile steel and GFRP tube. The formula for calculating the axial compressive capacity of these two types of columns by the superposition method can be given respectively by

$$N_{c1} = \eta\varphi(f_{fc}A_c + f_{fy}A_f) \tag{15}$$

$$N_{c2} = \eta\phi\left(f_{fc}A_c + f_{sr}A_s + f_{fy}A_f \right) \tag{16}$$

$$\eta = 1 - 0.1108r \tag{17}$$

$$\varphi = -0.163\ln(\lambda) + 1.377 \tag{18}$$

where η is the reduction coefficient of RCA replacement percentage on the axial compressive capacity of the columns, φ is the reduction coefficient of the slenderness ratio on the axial bearing capacity of the columns, which can be obtained through the regression fitting analysis on the test data, r is the RCA replacement percentage, and λ is the slenderness ratio of the composite columns.

4.6 Verification of calculations on the axial bearing capacity of the composite columns

The axial compressive capacity of the RAC filled GFRP tube columns and RAC filled GFRP tube-profile steel composite columns can be calculated by using Eqs. (15) and (16), respectively. Table 5 shows the comparison of the calculated and tested axial bearing capacities of the composite columns. The ratio of the calculated value N_c to the experimental value N_t is 0.99 on average and the standard deviation is 0.016. This indicates that the calculated values using Eqs. (15) and (16) are in fairly good agreement with the test results, which verifies the validity of the formulas to a certain extent.

5. Conclusions

In this study, the mechanical performances of 18 composite columns composed of the GFRP tube, RAC material and profile steel under the axial compression loads were investigated in detail through the static tests. The following conclusions can be drawn:

- The glass fibers of the GFRP tube were usually pulled off near the middle of the columns under axial compressive loads, resulting in the final failure of the RAC filled GFRP tube columns. In addition, the profile steel yielded first in the RAC filled GFRP tube columns-profile steel composite columns, then the internal RAC was crushed, and finally the glass fibers in the GFRP tube were torn until the columns lost their axial bearing capacity. Especially, the existence of the profile steel in the composite columns can improve the axial bearing capacity of columns significantly, and can delay the failure rate of the columns under axial loads.
- The axial bearing capacity of the RAC filled GFRP tube columns decreased gradually with the increase of

the RCA replacement percentage and the slenderness ratio based on the test results, and the maximum decreasing amplitudes were 11.1% and 21.5%, respectively. However, due to the presence of profiled steel in the columns, the decrease in the axial bearing capacity of the RAC filled GFRP tube-profiled steel composite columns with the increase of RCA replacement percentage or slenderness ratio was reduced markedly, and the maximum reductions were only 9.78% and 9.55%, respectively.

• The increasing RAC strength or profile steel ratio contributed to the axial compressive capacity of the composite columns and the maximum increase amplitudes were 6.1% and 14.17%, respectively. In addition, the increase of profile steel ratio can also properly improve the deformability of the columns, while increasing the strength of RAC material is disadvantageous to the deformability of the columns.

• The restraint ability of the GFRP tube to the internal RAC in the columns was weak at the beginning of loading. With the increase of axial loads, the transverse strain of the GFRP tube increased rapidly, which means that the restraint effect on the internal RAC increased and the RAC material was in a three-dimensional stress state. The compressive strength and deformation ability of the RAC material in the columns were effectively improved. In addition, in the RAC filled GFRP tube-profile steel composite columns, the strain growth rate of the profile steel was faster than that of the GFRP tube, which indicates that the profile steel yielded first and was brought into full play in the columns

• Based on the superposition method of the contribution of the axial bearing capacity of each part in the composite columns, the formulas for calculating the axial bearing capacity of columns were proposed, which considered the adversely effect of RCA replacement percentage and slenderness ratio. Although the calculated results are in good agreement with the experimental results, more experimental investigations are still needed to verify the validity of the above formulas.

Acknowledgments

The research was financially supported by the National Natural Science Foundation of China P.R. (No.51408485), The Project Supported by Natural Science Basic Research Plan in Shaanxi Province of China (No. 2019JM-193), and the Plan Projects of the Department of Housing and Urban-rural Development of Shaanxi Province (No.2015-K129) which is gratefully acknowledged.

References

Cardoso, R., Silva, R.V., Brito, J. and Dhir, R. (2016), "Use of recycled aggregates from construction and demolition waste in geotechnical applications: a literature review", *Waste. Manage.*, **49**(3), 131-145. https://doi.org/10.1016/j.wasman.2015.12.021.

Chen, Z.P., Xu, J.J., Chen, Y.L. and Su, Y.S. (2016), "Seismic behavior of T-shaped steel reinforced high strength concrete short-limb shear walls under low cyclic reversed loading", *Struct. Eng. Mech.*, **57**(4), 681-701. http://dx.doi.org/10.12989/sem.2016.57.4.681.

Desprez, C., Mazars, J., Kotronis, P. and Paultre, P. (2013), "Damage model for FRP-confined concrete columns under cyclic loading", *Eng. Struct.*, **48**(3), 519-531. https://doi.org/10.1016/j.engstruct.2012.09.019.

Eid, R. and Paultre, P. (2017), "Compressive behavior of FRP-confined reinforced concrete columns", *Eng. Struct.*, **132**(1), 518-530. https://doi.org/10.1016/j.engstruct.2016.11.052.

Gulsan, M.E., Jawahery A, Mohammed S. and Alshawaf, A.H. (2018), "Rehabilitation of normal and self- compacted steel fiber reinforced concrete corbels via basalt fiber", *Adv. Concrete Constr.*, **6**(5), 423-463. https://doi.org/10.12989/acc.2018.6.5.423.

Hadi, M.N.S., Wang, W. and Sheikh, M.N. (2015), "Axial compressive behaviour of GFRP tube reinforced concrete columns", *Constr. Build. Mater.*, **81**(15), 198-207. https://doi.org/10.1016/j.conbuildmat.2015.02.025.

Hosseinpour, F. and Abdelnaby, A.E. (2017), "Fragility curves for RC frames under multiple earthquakes", *Soil. Dyn. Earthq. Eng.*, **98**(7), 222-234. https://doi.org/10.1016/j.soildyn.2017.04.013.

Kara, I.F. (2016), "Flexural performance of FRP- reinforced concrete encased steel composite beams", *Struct. Eng. Mech.*, **59**(4), 775-793. https://doi.org/10.12989/sem.2016.59.4.775.

Kelly A. and Mileiko S.T. (1983), *Fabrication of Composites*, Handbook of Composites, North-Holland.

Li, P. and Wu, Y.F. (2015), "Stress-strain model of FRP confined concrete under cyclic loading", *Compos. Struct.*, **134**(15), 60-71. https://doi.org/10.1016/j.compstruct.2015.08.056.

Liang, J.F., Wang, E., He, C.F. and Hu, P. (2018), "Mechanical behavior of recycled fine aggregate concrete after high temperature", *Struct. Eng. Mech.*, **65**(3), 343-348. https://doi.org/10.12989/sem.2018.65.3.343.

Ma, H., Xue, J.Y., Liu, Y.H. and Dong, J. (2016), "Numerical analysis and horizontal bearing capacity of steel reinforced recycled concrete columns", *Steel Compos. Struct*., **22**(4), 797-820. https://doi.org/10.12989/scs.2016.22.4.797.

Mesbah, H.A. and Benzaid, R. (2017), "Damage-based stress-strain model of RC cylinders wrapped with CFRP composites", *Adv. Concrete Constr.*, **5**(5), 539-561. https://doi.org/10.12989/acc.2017.5.5.539.

Mykolas, D., Juozas, V., Artūras, B., Tomas, S. and Marius, B. (2013), "Experimental investigation of the load carrying capacity of eccentrically loaded reinforced concrete elements strengthened with CFRP", *Procedia Eng.*, **57**(1), 232-237. https://doi.org/10.1016/j.proeng.2013.04.032.

Rosado, L.P., Vitale, P., Penteado, C.S.G. and Arena, U. (2017), "Life cycle assessment of natural and mixed recycled aggregate production in brazil", *J. Clean. Prod.*, **151**(10), 634-642. https://doi.org/10.1016/j.jclepro.2017.03.068.

Samaan, M. and Mirmiran, A. (1998), "Model of concrete confined by fiber composites", *J. Struct. Eng.*, **124**(9), 1025-1031. https://doi.org/10.1061/(ASCE)0733-9445(1998)124:9(1025).

Saravanakumar, P. and Dhinakaran, G. (2013), "Durability characteristics of recycled aggregate concrete", *Struct. Eng. Mech.*, **47**(5), 701-711. https://doi.org/10.1016/j.conbuildmat.2012.11.106.

Senaratne, S., Lambrousis, G., Mirza, O., Tam, V.W.Y. and Kang, W.H. (2017), "Recycled concrete in structural applications for sustainable construction practices in Australia", *Procedia Eng.*, **180**, 751-758. https://doi.org/10.1016/j.proeng.2017.04.235.

Tabsh, S.W. and Abdelfatah, A.S. (2009), "Influence of recycled concrete aggregates on strength properties of concrete", *Constr. Build. Mater.*, **23**(2), 1163-1167.

https://doi.org/10.1016/j.conbuildmat.2008.06.007.
Thomas, C., Setién, J., Polanco, J.A., Alaejos, P. and Juan, M. S.D. (2013), "Durability of recycled aggregate concrete", *Constr. Build. Mater.*, **40(**3), 1054-1065. https://doi.org/10.1016/j.conbuildmat.2012.11.106.
Xiao, J.Z. and Huang, Y.J. (2012), "On the seismic behavior and damage assessment of recycled aggregate concrete filled GFRP tube column", *China Civil Eng. J.*, **45**(11), 112-120. (in Chinese)
Xiao, J.Z., Li, W.G., Fan, Y.H. and Huang, X. (2012), "An overview of study on recycled aggregate concrete in China (1996-2011)", *Constr. Build. Mater.*, **31**(6), 364-383. https://doi.org/10.1016/j.conbuildmat.2011.12.074.
Xiong, Z., Deng, J.P., Liu, F., Li, L.J. and Feng, W.X. (2018), "Experimental investigation on the behavior of GFRP- RAC-steel double-skin tubular columns under axial compression", *Thin. Wall. Struct.*, **132**(11), 351-360. https://doi.org/10.1016/j.tws.2018.08.026.
Xu, J.J., Chen, Z.P., Xiao, Y., Demartino, C. and Wang, J.H. (2017), "Recycled aggregate concrete in FRP-confined columns: a review of experimental results", *Compos. Struct.*, **174**(15), 277-291. https://doi.org/10.1016/j.compstruct.2017.04.034.
Youssef, M.A., Meshaly, M.E., Elansary, A.A., Youssef, M.A., Meshaly, M.E. and Elansary, A.A. (2017), "Ductile corrosion-free GFRP-stainless steel reinforced concrete elements", *Compos. Struct.*, **182**(9), 1-25. https://doi.org/10.1016/j.compstruct.2017.09.037.
Yu M.H. (2004), *Unified Strength Theory and its Applications*, Springer-Verlag, Berlin, Heidelber.
Zeng, J.J., Guo, Y.C., Gao, W.Y., Li, J.Z. and Xie, J.H. (2017), "Behavior of partially and fully FRP-confined circularized square columns under axial compression", *Constr. Build. Mater.*, **152**(10), 319-332. https://doi.org/10.1016/j.conbuildmat.2017.06.152.
Zeng, L., Li, L.J., Su, Z. and Liu, F. (2018). "Compressive test of GFRP-recycled aggregate concrete-steel tubular long columns", *Constr. Build. Mater.*, **176**(7), 295-312. https://doi.org/10.1016/j.conbuildmat.2018.05.068.

JK